Using the Multi-Loop Fault Analysis Method for Setting and Evaluating Generator Protection Elements

Ritwik Chowdhury, Dale Finney, and Normann Fischer
Schweitzer Engineering Laboratories, Inc.

This paper was presented at the 71st Annual Conference for Protective Relay Engineers and can be accessed at: https://doi.org/10.1109/CPRE.2018.8349835.

For the complete history of this paper, refer to the next page.

Published in
Synchronous Generator Protection and Control: A Collection of Technical Papers Representing Modern Solutions, 2019

Previously presented at the
71st Annual Conference for Protective Relay Engineers, March 2018

Originally presented at the
44th Annual Western Protective Relay Conference, October 2017

Using the Multi-Loop Fault Analysis Method for Setting and Evaluating Generator Protection Elements

Ritwik Chowdhury, Dale Finney, and Normann Fischer, *Schweitzer Engineering Laboratories, Inc.*

***Abstract*—Stator winding interturn, interbranch, and series faults can result in large circulating currents in the faulted coils. Generator protection elements may not be sensitive enough to detect these fault conditions until the fault evolves into a phase-to-phase or phase-to-ground fault. Large machines have been severely damaged by delayed or failed protection system operation. Determining fault quantities for the various possible internal faults is not trivial and requires the aid of numerical models. Protection element models can then be used to determine the protection coverage provided by these elements.**

Certain machine modeling methods are useful for analyzing external faults or power system transients but are not appropriate for analyzing internal faults. The most commonly used machine models use *dq0* transformation and assume an ideal equivalent model of the machine derived from its normal operating mode using lumped winding parameters. Consequently, these models ignore the effect of the strong harmonics that result from the internal machine asymmetry during internal faults. Alternate methods, such as symmetrical component analysis or phase-coordinate methods, are simplified models that introduce large errors during internal asymmetric conditions.

The multi-loop method treats a machine as a set of loops in relative motion. The method involves a permeance analysis of the machine to calculate the time-variant electric parameters of the stator branches and rotor loops. The stator branches (including fault branches) are converted to loops via a transformation matrix corresponding to the state of the machine. The model is then solved using a numerical method. Because the multi-loop method uses machine geometry and winding design information, it preserves the harmonics that result from internal faults. The transformation matrix provides a simple and intuitive mechanism to apply internal faults in the fractional winding.

In this paper, we validate the multi-loop method using test data from a scale-model machine in a lab. We then use the fault quantities obtained from the multi-loop method to determine the sensitivity and coverage provided by various generator internal-fault protection algorithms for the lab machine.

I. Introduction

An examination of the physical layout of a stator winding provides an indication of where faults are most likely to occur and the types of those faults. Most faults are phase-to-ground or phase-to-phase. Ground fault and differential schemes are relied on to rapidly identify and isolate these faults. In some windings, interturn or interbranch faults are possible. For instance, interturn faults are possible in windings that are constructed from multi-turn coils. Although the current through the winding can be relatively small, the current in the shorted turn can be several times nominal.

A series fault can result from a bar fracture (caused by high vibration, for example) or the failure of a welded or bolted connection [1]. Often a portion of the winding conductor is vaporized before the insulation is breached [2]. Neither interturn nor series faults are detected by differential schemes because there is no difference in the currents at each end of the winding. While these faults are theoretically detectable by ground fault protection (for example, a neutral overvoltage element), it is often not possible to set the element sensitively enough to provide effective protection.

The first step in a fault survey is to examine the layout of the winding to identify possible failure locations. From this, the possible fault types and required type of protection can be determined. Ideally, by obtaining the fault currents and voltages for the potential fault points, the worst-case operating quantities can be determined. These can then be used to optimize the protection element settings.

For most internal-fault types, there are no good analytical methods for empirical calculation of fault currents and voltages. Research into numerical methods for internal-fault calculation extends back almost to the time when digital computers first became commercially available.

Park, Krause, and others have developed reference frame transformations that have generally become known as *dq0* models [3] [4]. These models assume a sinusoidal spatial distribution of the stator winding magnetomotive force (MMF), which greatly simplifies the development of machine models. These transformations are accurate for a fault at the generator terminals or external faults but, in their original formulations, cannot be applied for faults within the winding.

Several internal-fault calculation models have been described in [5]–[19]. The following observations can be made about these methods:

- Most of these methods replace the sinusoidal spatial distribution of the MMF with a winding function. The use of a winding function facilitates modeling of the harmonics corresponding to internal faults. Some generator protection functions make use of these harmonics.
- Most internal-fault models account for the nonuniform air gap found in salient-pole machines.
- Some internal-fault models seek to derive the model parameters from the operational parameters of the machine (X_d, X_q, X'_d, and so on). Others require more detailed information about the winding (pitch factor, distribution factor, and so on).
- Internal-fault models can be characterized in terms of the types of faults they can simulate (phase-to-ground, phase-to-phase, interturn, interbranch, and series).

- Some internal-fault models have been developed specifically for integration into real-time digital simulators [17] [18] [19]. Numerical efficiency is given a higher priority in these formulations.

In general, internal-fault models are more complex than the *dq0* models. However, once implemented and validated, internal-fault models provide valuable insights, as we will demonstrate.

II. The Multi-Loop Method

The multi-loop method was developed and popularized by Gao [5]. It considers the geometry of the winding and allows each individual coil and branch of the winding to be modeled. The approach requires detailed winding information, but it allows all fault types to be modeled. It also allows branches to be grouped for the evaluation of split-phase or transverse differential protection schemes. In this section, we only present the equations that allow a functional understanding of the method. The details and derivations are available in [5].

A. Permeance Model

In a magnetic circuit, the flux produced by the MMF takes the path of highest permeance (least reluctance) through the circuit and is the fundamental method of electromechanical energy conversion in an electric machine. The permeance coefficient (λ_δ) in a rotating machine is primarily facilitated by the air gap and is a function of the air-gap length (δ) between the rotor and stator. In salient-pole machines, the air-gap length is not uniform. Fig. 1 shows a cross section of a salient pole machine.

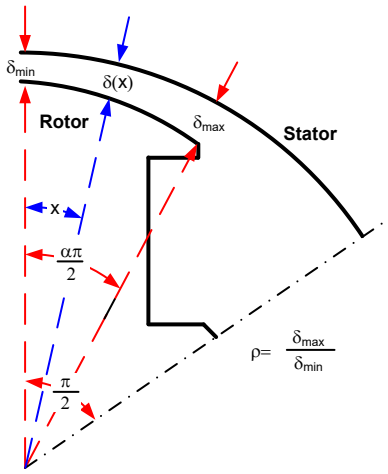

Fig. 1. Air-gap length, δ(x), as a function of the position (x) of a salient-pole rotor spanning απ/2 electrical radians

Due to the symmetry of the air-gap length for a pole pair, λ_δ can be represented with a Fourier series with even harmonics.

$$\lambda_\delta(x) = \frac{\lambda_0}{2} + \sum_l \lambda_{2l} \cos(2lx); l = 1, 2, \ldots \quad (1)$$

The development of (1) and its coefficients (λ_0 and λ_{2l}) are included in Appendix A. Fig. 2 shows an example of the air-gap permeance for a salient-pole machine.

The performance of the permeance model has an expected sharp drop in the interpolar space. This is nearly identical to the results obtained from finite element analysis, as described in [20]. A cylindrical rotor can be modeled as a special case of the salient-pole rotor with a uniform air-gap length.

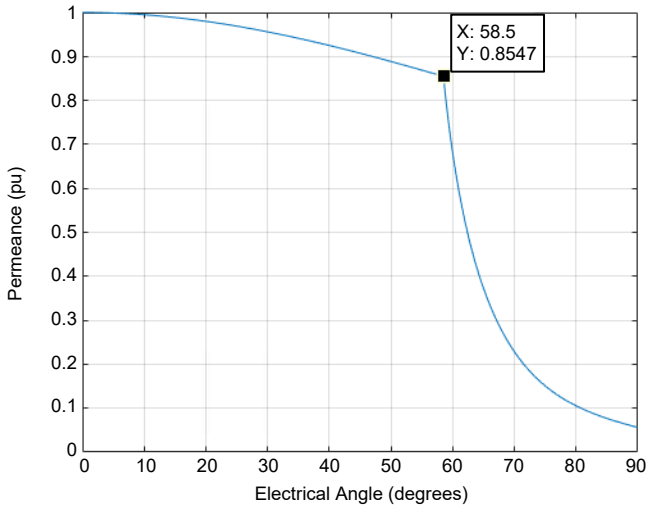

Fig. 2. Normalized permeance model of a salient-pole rotor

We consider air-gap expansion caused by the slot effect via Carter's coefficient [4] but ignore slot harmonics. This analysis of permeance is not unique, and several of the methods mentioned in the Introduction use a similar approach. The permeance coefficients correspond to the harmonic sources in a rotating machine.

B. Circuit Parameters Using a Winding Function

The multi-loop method treats a coil as the basic element of a winding. The coil resides in a stator slot and has one or more turns. The current through the coil creates a square-wave MMF, which can be represented as a sum of cosine terms via Fourier analysis. This MMF (F) has a resultant flux density (B) through the permeance path (λ) provided by the air gap (δ), as shown in (2).

$$B = F \bullet \lambda \quad (2)$$

As discussed previously, the permeance model accounts for the nonuniformity of the air gap and is represented as a Fourier series. Consequently, the resultant flux density is also a Fourier series with time-variant coefficients that account for the rotor position and relative coil position.

Inductance is the ratio of flux linkage (ψ) to per-unit current (i). The self-inductance (L) of a coil is the flux linkage of the coil that is due to its own current, and the mutual inductance (M) is the flux linkage of the coil that is due to current in a different coil. Flux linkage accounts for the surface area (S) and number of turns (w).

$$\psi = w \int B \, dS \quad (3)$$

A branch consists of several coils connected in series either in the stator or rotor winding. All coils in a branch carry the same current, so equivalent branch inductances can be derived. For instance, the mutual inductance between the field and a stator phase branch (ϕ_1) can be represented by Equations (4)–(7).

$$M_{\phi_i fd} = \frac{2 w w_{fd} \tau l}{\pi a_{fd}} \sum_k \frac{\lambda_{dk}}{k} \bullet k_{wk} \bullet \cos\left(k \bullet (\gamma + \alpha)\right) \quad (4)$$

$$k_{wk} = k_{yk} \bullet k_{pk} \quad (5)$$

$$k_{yk} = \sin\left(k \bullet \beta \bullet \frac{\pi}{2}\right); k_{pk} = \frac{\sin\left(q \bullet k \bullet \frac{\theta}{2}\right)}{q \bullet \sin\left(k \bullet \frac{\theta}{2}\right)} \quad (6)$$

$$\tau = \frac{\pi \bullet R}{P}; k = 1, 3, \ldots \quad (7)$$

The turn information required to obtain the flux linkage is provided by the following values:

- w is the number of turns per stator branch.
- w_{fd} is the number of field turns per pole.
- a_{fd} is the number of parallel branches in the field winding.

The permeance information corresponding to the orientation is provided by the following values:

- k is the harmonic order per the Fourier series.
- λ_{dk} is the direct-axis permeance coefficient produced by the kth-harmonic MMF, obtained similarly to λ_{2l}.
- γ is the electric lead angle between the rotor reference (d-axis) and the stator coordinate axis.
- ϕ is the phase of the branch under consideration.
- α is the angle associated with the phase (ϕ).

The winding information is provided by the following values:

- β is the stator pitch ratio. This is the ratio of the pitch of a stator coil (coil span) with respect to the pole pitch.
- k_{yk} is the stator pitch factor.
- q is the number of coils per coil group. This can be calculated as the number of slots per pole per phase.
- θ is the electrical angle per stator slot. This can be calculated as 180 degrees divided by the number of slots under a pole.
- k_{pk} is the distribution factor.
- k_{wk} is the winding factor, containing both the pitch (k_{yk}) and winding distribution (k_{pk}) information.

The winding information is easily obtained from a winding diagram. An example stator winding diagram is shown in Appendix D.

The geometry information is provided by the following values:

- τ is the pole pitch of the machine. This accounts for the stator inner radius (R) and the number of pole pairs (P).
- l is the length of the stator iron.

The multi-loop method preserves important details corresponding to the geometry and winding information of the machine. Doing so provides attenuation for the different harmonic orders of the permeance coefficient obtained in Section II, Subsection A.

The multi-loop method derives the various machine self- and mutual-inductances using the principles discussed. The details can be found in [5]. This approach is not unique and several methods mentioned in the Introduction use a similar approach.

C. *Solving the Circuit Using Loop Analysis*

Once the inductance parameters are obtained, the machine can be represented using branch circuit equations, as shown in (8). The expanded terms are shown in Fig. 3, and the associated circuit is shown in Fig. 4.

$$U = p(LI) + RI + V' \quad (8)$$

where:

U is the branch voltages.

L is the inductance parameters.

I is the branch currents.

p is the derivative operator (d/dt).

R is the resistance terms.

V' is the external system voltage source.

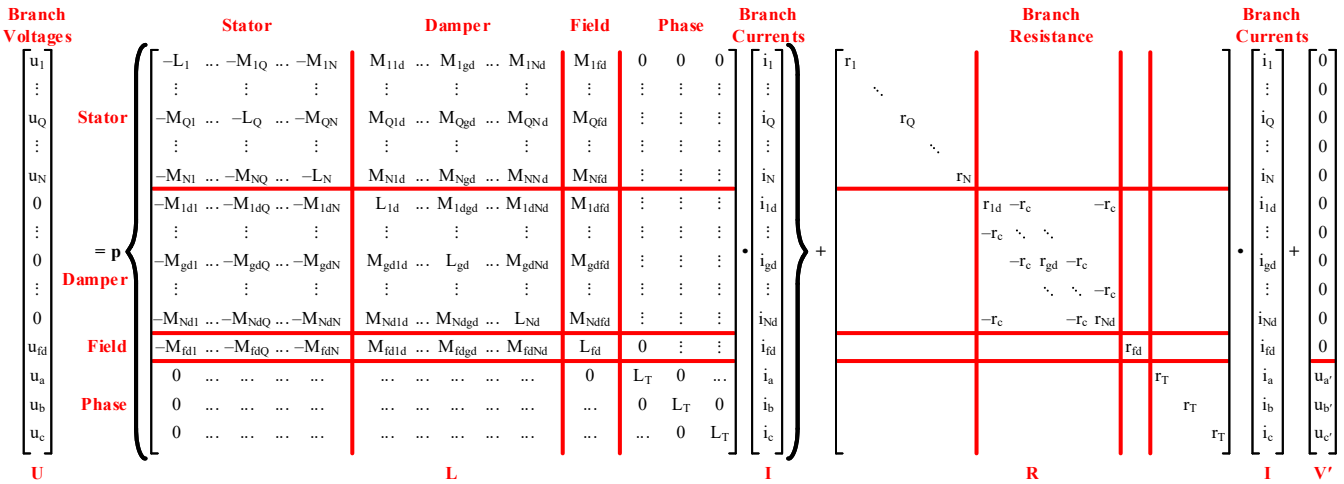

Fig. 3. Branch matrix describing the multi-loop system model

For example, the inductance matrix consists of stator, rotor, and system terms. The parameters of each stator branch (1…Q…N) and damper loop (1d…gd….Nd) can be obtained from Section II, Subsection A, demonstrating the extent of the detail available from the permeance model. In our model however, the damper terms are missing, hence we incur a reduction of order of the equations.

After the branch circuit equations are identified, the defining step of the multi-loop method is the conversion from branches to loops, where the sum of the voltage around a loop is zero [5]. The circuit corresponding to this branch-to-loop conversion is shown in Fig. 4 with the different fault types.

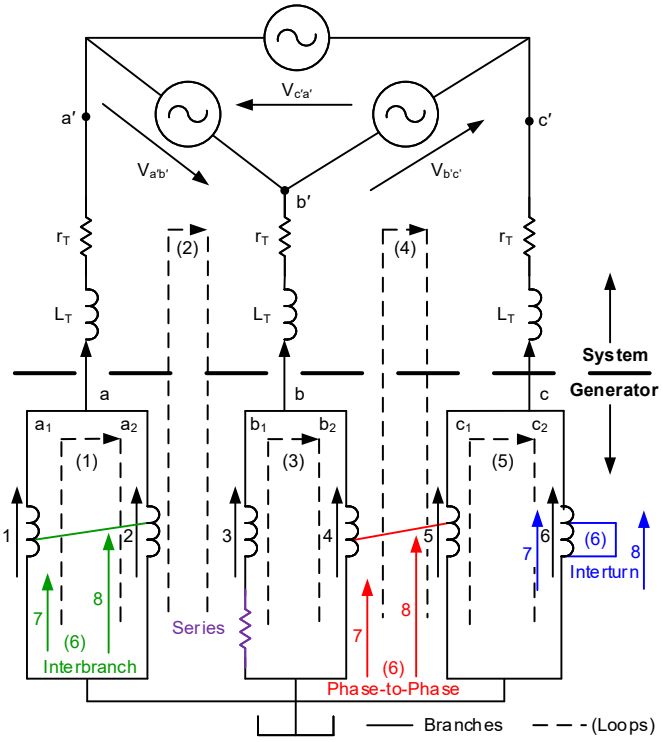

Fig. 4. Multi-loop circuit

The process of conversion from branches to loops is associated with a transformation matrix (H) such that the sum of the voltage around a loop is zero. For instance, the loop voltages (U′) and loop currents (I′) are related to the branch voltages (U) and branch currents (I) by (9) and (10).

$$U' = HU \tag{9}$$

$$I = H^T I' \tag{10}$$

Pre-multiplying the circuit equation by the transformation matrix results in (11) and (12).

$$HU = HLpI + HpLI + HRI + HV' \tag{11}$$

$$U' = HLH^T pI' + HpLH^T I' + HRH^T I' + HV' \tag{12}$$

Substituting $L' = HLH^T$ and $R' = pL' + HRH^T$ results in the loop circuit equation (13).

$$U' = L'pI' + R'I' + HV' \tag{13}$$

Because the loop currents are the state variables, rearranging (13) results in the state equation of the synchronous generator shown in (14).

$$pI' = L'^{-1}\left(U' - R'I' - HV'\right) = -L'^{-1}R'I' + L'^{-1}\left(U' - HV'\right) \tag{14}$$

The state equation is a first-order ordinary differential equation that can be solved via an iterative method, such as Runge-Kutta, and is represented by (15).

$$pI' = A_1 I' + A_0 \tag{15}$$

where:

$$A_1 = -L'^{-1}R' \tag{16}$$

$$A_0 = L'^{-1}\left(U' - HV'\right) \tag{17}$$

During phase-to-phase, interbranch, and interturn faults, the order and number of branches increases by two with respect to normal operation. Subsequently, we add one more loop equation that describes the electrical coupling of the faulted stator loop with the other stator loops (see the different Loop 6 options in Fig. 4, which depend on the fault type). This approach is slightly different from that in [5], where only one additional branch and loop is added for interturn faults.

During series faults, the number of branches and loops does not increase; only the circuit parameters change via the addition of a series resistance on the faulted branch. External faults and the generator grounding impedance are provided by the 3 x 3 external terms of the impedance matrices (see L_T and r_T in Fig. 3 and Fig. 4)

We consider the effect of core saturation by using the method in Appendix B. We simplify the multi-loop model to consider the most dominant parameters. The field circuit is represented with a Thévenin equivalent voltage source with the controls deactivated. The governor control is deactivated as well, and the rotor maintains synchronous speed. Damper windings are not modeled. This simplification did not have a significant impact on our simulation accuracy, as shown in Section III, but we plan to address this deficiency in the future.

III. Model Validation

To validate our model of the multi-loop method, we compared our results with measured data from a small 18 kVA, scale-model, solidly grounded, salient-pole generator with a motor as the prime mover, as shown in Fig. 5. The machine data are provided in Appendix C.

Fig. 5. 18 kVA, 6-pole machine used for multi-loop model

The model was validated by verifying events with two types of loads, as well as both internal and external faults by deactivating both the excitation and the governor control. This section examines the behavior for the two loading conditions, one with an external phase-to-phase fault applied and the other with an internal interturn fault applied.

A. External Fault

While the generator was loaded with a 6 A wye-grounded resistive load bank, a BC fault was applied. The comparison of the scale-model machine and the simulation responses in Fig. 6 shows that they are in close agreement.

B. Interturn Fault

The generator was loaded by synchronizing it to an external power system. A turn-to-turn fault spanning five turns was applied on Phase A near the generator neutral terminal. A comparison of the phase currents from the scale-model machine and the simulation is shown in Fig. 7.

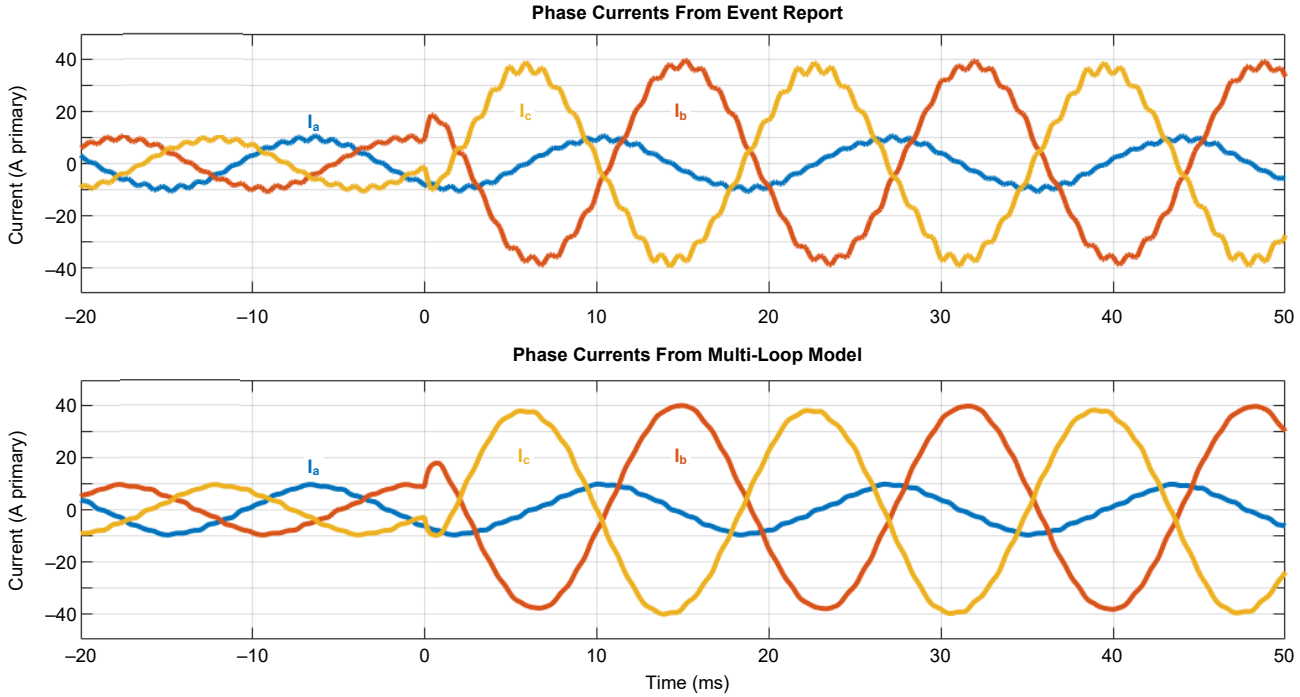

Fig. 6. Response comparison between the scale-model machine (top) and the simulation (bottom) for an external phase-to-phase fault

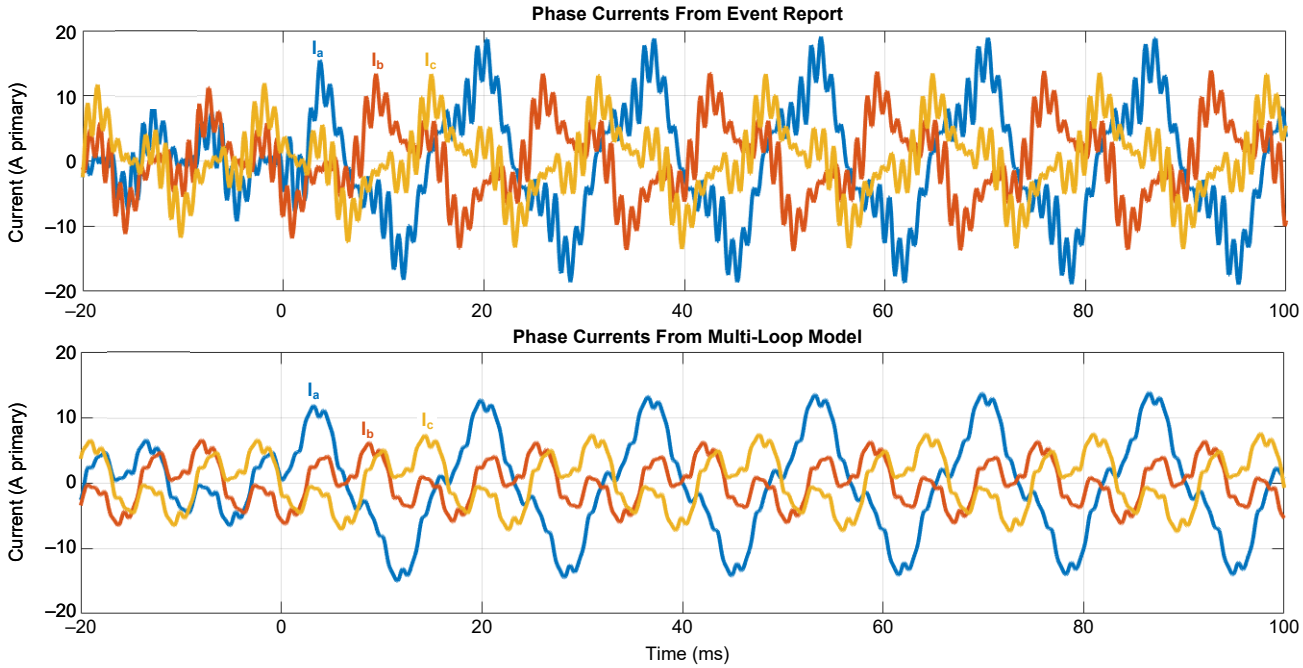

Fig. 7. Response comparison between the scale-model machine (top) and the simulation (bottom) for a five-turn interturn fault

A comparison of the harmonics of the faulted phase currents corresponding to the interturn fault (Fig. 7) is shown in Fig. 8. The accuracy is good for the lower-order harmonics. The significant higher-order harmonics (e.g., the seventeenth harmonic) are caused by slot harmonics that we did not model.

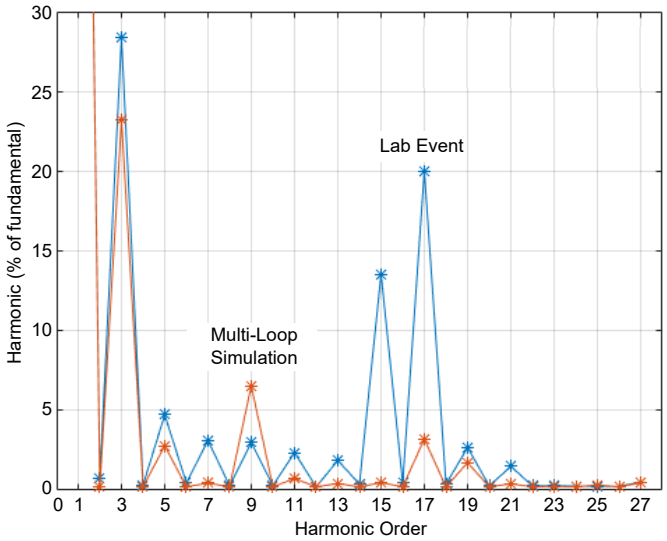

Fig. 8. Comparison of the harmonics between the experiment (blue) and the simulation (red) for a five-turn Phase A interturn fault

The measured circulating fault current for the five-turn fault was more than 7 pu (330 A) of the machine rated current, which demonstrates the severity of this condition. The fault current does not manifest itself in the phase currents and cannot be seen in Fig. 7, demonstrating the challenging sensitivity requirement for protection. Based on our lab test results, the five-turn fault generates a larger amount of circulating fault current than a one-turn (2.8 pu) or a ten-turn (4.5 pu) interturn fault, i.e., the behavior is nonlinear.

Protection schemes need to be designed with sufficient sensitivity to allow the detection of these types of faults reliably; otherwise, a fault can go undetected and cause considerable damage before it evolves into a phase-to-ground or phase-to-phase fault. If sensitive protection is not provided, local heating caused by the high fault current can present a fire hazard [21] [22]. Machine damage due to internal faults can result in costly repairs and lost revenue caused by downtime in the order of $100 million, as seen from stator-winding failures from numerous large units [2].

IV. Evaluation of Generator Protection Elements

A. Machine Fault Survey

To evaluate the protection coverage provided to a machine by the protection elements, we performed a survey of the possible faults in the end-winding region and slots, as shown in Fig. 9, Fig. 10, and Fig. 11. This method, including the survey and application of the multi-loop method, has been used to design optimal protection schemes for two different types of machines in the Three Gorges generating plant [12] [16].

The benefit of the survey is that it only considers faults that are plausible and not those that are practically unlikely to occur because of the machine's construction. The possible fault locations in the end-winding region, for instance, depend on the winding configuration, as shown in Fig. 9. We considered all shunt fault types that do not involve the ground: interturn, interbranch, and phase-to-phase.

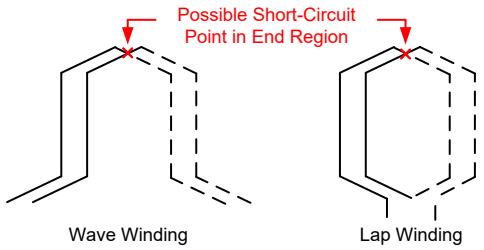

Fig. 9. Possible fault points in the end-winding region for wave and lap winding configurations

The possibility of a fault in the slot depends on the particulars of the winding. Stator windings are typically form-wound, multi-turn coils for smaller units and bars for larger units [23]. If the slot is occupied by two single-turn bars, as shown in Fig. 10, only phase-to-ground faults are expected.

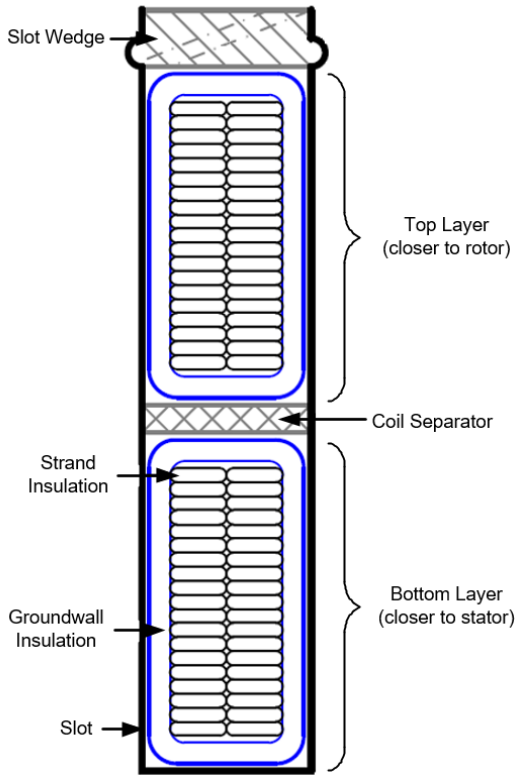

Fig. 10. Machine with Roebel bars on two layers separated by a Bakelite separator

If the slot consists of coils or bars with multiple turns, the possibility of an interturn fault in the slot exists, as shown in Fig. 11.

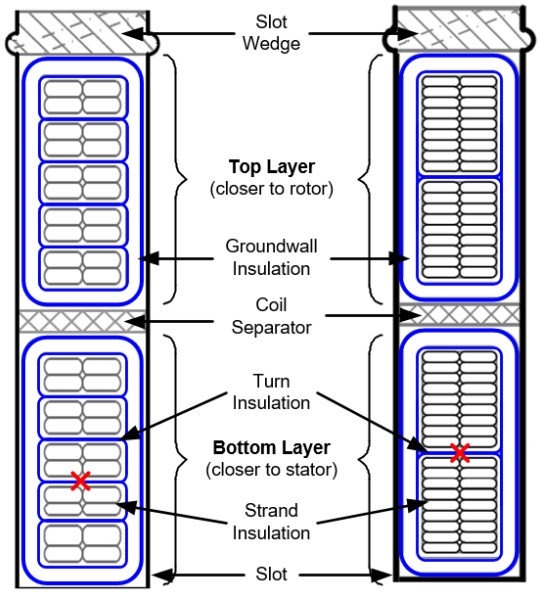

Fig. 11. Possible interturn fault locations in the slot for a machine with a form-wound multi-turn coil (left) or a two-turn Roebel bar (right)

The machine used in this study has a random-wound stator winding. This is typical for machines smaller than 1 MVA. The survey approach is the same as for a machine with form-wound coils and is described in Appendix D.

In addition to the survey, we considered the possibility of a series fault in the form of a cracked or broken conductor [2]. Although such a condition is unlikely for our machine, we included this fault type to evaluate protection element sensitivity by comparing the minimum series-fault resistances that the elements detect.

B. Protection Elements

This section discusses protection elements that are currently applied to detect stator phase faults and several other elements proposed in the literature. We did not include ground faults in the study because this fault type can be evaluated without a complex internal-fault model if the unit is high-impedance grounded.

The focus of this study was to determine protection sensitivity. Security is also an important protection consideration, but a security analysis does not require an internal-fault model. The pickup settings were chosen based on minimal instrument transformer and relay measurement errors (Appendix E) and sensitive settings guidelines provided by manufacturers. Fig. 12 shows a single-line diagram of the machine under study, including the location of the current and voltage measurements used by the various protection functions.

1) Generator Phase Differential Element

The generator phase differential element (87G) compares the phase currents at each end of the stator winding. We use the following equations to represent this element in the study.

$$87G_{\phi} = \left(I_{\phi DIF} > SLP \bullet I_{\phi RST}\right) \& \left(I_{\phi DIF} > PKP\right) \quad (18)$$

$$I_{\phi DIF} = \left|I_{\phi t} + I_{\phi n}\right| \quad (19)$$

$$I_{\phi RST} = \left|I_{\phi t}\right| + \left|I_{\phi n}\right| \quad (20)$$

$$SLP = 20\%;\ PKP_{MIN} = 10\% \quad (21)$$

2) Negative-Sequence Directional Element

The negative-sequence directional element (32Q) uses negative-sequence quantities to identify an unbalance event and indicate whether it is internal to the generator. This element has been used for generator protection, as discussed in [24] [25].

$$32QF = \left(Z_2 < Z_{2F}\right) \& \left(\left|V_2\right| > V_{2MIN}\right) \& \left(\left|I_2\right| > I_{2MIN}\right) \quad (22)$$

$$32QR = \left(Z_2 > Z_{2R}\right) \& \left(\left|V_2\right| > V_{2MIN}\right) \& \left(\left|I_2\right| > I_{2MIN}\right) \quad (23)$$

$$Z_2 = \frac{\mathrm{Re}\left(V_2 \bullet \left(I_2 \bullet e^{j\theta}\right)^*\right)}{\left|I_2\right|^2} \quad (24)$$

$$Z_{2F} = -0.3 \bullet Z_{2\_SYS};\ Z_{2R} = 0.3 \bullet Z_{2\_GEN} \quad (25)$$

$$V_{2MIN} = 1.0\%;\ I_{2MIN} = 2.0\%;\ \theta = 85° \quad (26)$$

We evaluated the negative-sequence impedance method [26] [27] with minimum V_2 and I_2 supervision to account for measurement errors. We set the forward threshold to 30 percent of the strongest system negative-sequence impedance to allow margin for nonhomogeneity. We set the reverse threshold at 30 percent of the generator Z_2 [28], which can be assumed to be 20 percent if this information is not available in the data sheet or via tests [29].

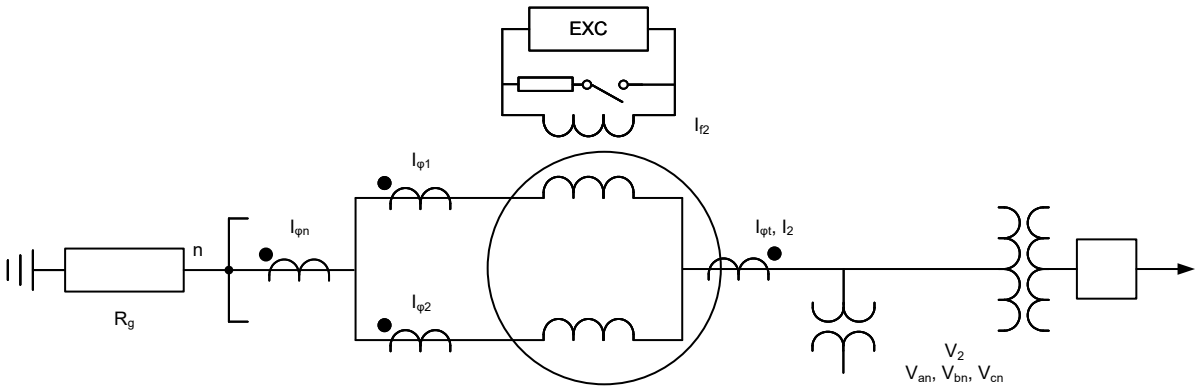

Fig. 12. Single-line diagram with instrument transformer signals used by protection functions

3) Unbalance Overvoltage Element

An unbalance overvoltage element (59GN) is commonly used outside North America to provide interturn fault protection. It is similar to the fundamental neutral overvoltage element (59N) but is more sensitive to internal faults that do not include the ground. The 59N element can be evaluated for interturn faults using simpler techniques, as is described in Appendix F.

A 59GN element measures the phase-to-neutral voltage unbalance. Three PTs are each connected from the phase to the star-point (neutral) of the machine via a high-voltage cable, and the PT secondary is connected via a broken-delta configuration [30]. The operating signal can also be derived from other methods that measure both the terminal and neutral voltages, such as a vector sum of the phase-to-ground and neutral-to-ground voltages [31]. In this study, we use the first method shown in (27) to obtain high sensitivity.

$$59GN = \left|V_{an} + V_{bn} + V_{cn}\right| > PKP\left(\text{Measured}\right) \quad (27)$$

$$59GN = \left|V_{ag} + V_{bg} + V_{cg} - 3V_{ng}\right| > PKP\left(\text{Calculated}\right) \quad (28)$$

$$PKP = 1.50\% \quad (29)$$

The pickup is set to 1.50 percent (see Appendix E) will likely not detect a single-turn fault. For our machine, we expect to detect a single-turn fault with a pickup less than 0.55 percent (depending on the system impedance), as calculated by the following equation when substituting 1 (single-turn) divided by the number of turns per phase:

$$PKP < \frac{N_{flt}}{N_{turn/branch} \bullet N_{branch/phase}} \quad (30)$$

4) Split-Phase Overcurrent Element

A split-phase overcurrent element (50SP) is applicable to machines with multiple branches, typically hydroelectric units. The standing circulating current in machines that is caused by manufacturing limitations rarely exceeds 0.5 percent for a well-balanced winding and is usually below 2 percent otherwise [21]. We modeled the manufacturing tolerance using scaling circuit parameters to obtain a standing circulating current of 0.4 percent. We use the following element definition:

Using the following pickup (PKP) definition, we set our pickup at 3.0 percent (considerably above the standing circulating current) to account for measurement errors:

$$50SP = \left|I_{\phi 1} - I_{\phi 2}\right| > PKP \quad (31)$$

$$PKP = 3.0\% \quad (32)$$

We assume that the element will be restrained during an external event, hence maintaining security without sacrificing sensitivity.

5) Split-Phase Transverse Differential Element

A split-phase transverse differential element (87SP) uses the branch current magnitudes to provide a restraint to the split-phase current. We used the following pickup definition:

$$87SP_{\phi}\left(I_{\phi DIF} > SLP \bullet I_{\phi RST}\right) \& \left(I_{\phi DIF} > PKP\right) \quad (33)$$

$$I_{\phi DIF} = \left|I_{\phi 1} - I_{\phi 2}\right|;\ I_{\phi RST} = \left|I_{\phi 1}\right| + \left|I_{\phi 2}\right| \quad (34)$$

$$SLP = 20\%;\ PKP = 10\% \quad (35)$$

We set the pickup and slope with the most sensitive settings available from the relay manufacturers [24] [25].

6) Stator Field Differential Element

A stator field differential element (87SF) implements a differential between the second harmonic in the field current and the negative sequence in the terminal phase currents [32]. It uses N_{SF} as the transformation ratio corresponding to external unbalanced events and θ_C as the compensation angle.

$$87SF = \left(I_{DIF} > SLP \bullet I_{RST}\right) \& \left(\left|I_{f2}\right| > I_{f2MIN}\right) \& \left(\left|I_2\right| > I_{2MIN}\right) \quad (36)$$

$$I_{DIF} > \left|I_{2(60Hz)} + N_{SF} \bullet I_{f(60Hz)} \bullet e^{-j\theta c}\right| \quad (37)$$

$$I_{RST} > \left|I_{2(60Hz)}\right| + \left|N_{SF} \bullet I_{f(60Hz)} \bullet e^{-j\theta c}\right| \quad (38)$$

$$SLP = 20\%;\ I_{fMIN} = 0.2\%;\ I_{2MIN} = 2.0\% \quad (39)$$

7) I_{f2} and P_{2t} Element

The following method was proposed to detect internal asymmetric conditions using the second-harmonic field current as the operating quantity and the negative-sequence real power in the stator as the restraining quantity [33]. The following function uses a constant threshold for both the second-harmonic field current and the negative-sequence power:

$$67PF = \left(\left|I_{f2}\right| > I_{f2MIN}\right) \& \left(\text{Re}\left(-V_2 \bullet I_2^{*}\right) > P_{2MIN}\right) \quad (40)$$

$$I_{f2MIN} = 0.2\%;\ P_{2MIN} = 0.05\% \quad (41)$$

The pickup for I_{f2} is limited by the sensitivity of the transducer (see Appendix E), and the pickup for the power threshold (P_{2MIN}) is set to a reasonable value [34].

Using P_2 makes this function less sensitive when the external system is more inductive (less resistive). An alternate would be to use Q_2, as follows:

$$67QF = \left(\left|I_{f2}\right| > I_{f2MIN}\right) \& \left(\text{Im}\left(-V_2 \bullet I_2^{*}\right) > Q_{2MIN}\right) \quad (42)$$

$$I_{f2MIN} = 0.02\%;\ Q_{2MIN} = 0.05\% \quad (43)$$

Q_2 is essentially a torque-based 32Q element with a constant threshold. This element effectively becomes a negative-sequence directional overcurrent element operating on the second-harmonic field current.

C. Protection Performance With Respect to Survey

We used the internal-fault model validated in Section III for a fault study. We followed the fault survey procedure in Section IV, Subsection A to identify the various fault types and locations for the study. The results in this section are for a model of the lab machine using the protection element settings from Section IV, Subsection B. For other machines, the performance of the elements is expected to vary depending on the machine, system, and load.

1) Phase-to-Phase Faults

The fault survey (Appendix D) identified a total of 450 possible phase-to-phase fault locations. We applied faults at these locations and checked the protection operation. The results are shown in Table I.

TABLE I
PHASE-TO-PHASE FAULT RESULTS

Element	Number of Faults Detected (higher is better)
87G	439
32Q	450
59GN	450
50SP	450
87SP	450
87SF	450
67QF	446

The results in Table I can be summarized as follows:

- 32Q, 59GN, 50SP, 87SP, and 87SF provide 100 percent coverage of the winding for this system when using the chosen sensitive settings.
- 67QF and 87G both detected most of the faults. Both elements are unable to detect some faults near the neutral because of their sensitivity limits.
- 87G, 50SP, and 87SP are the only functions that can reliably detect internal three-phase faults.

2) Interturn Faults

We applied interturn faults and checked the protection operation. The number of shorted turns was varied from 1 to 10 to simulate interturn faults in the slot. The results are shown in Table II.

TABLE II
SLOT INTERTURN FAULT RESULTS

Element	Number of Shorted Turns Detected (lower is better)
87G	NA
32Q	6
59GN	3
50SP	6*
87SP	10*
87SF	3
67QF	10

*Element gains or loses sensitivity depending on faulted branch because of steady-state asymmetry introduced by manufacturing tolerance.

None of the elements is sensitive enough to detect a single-turn fault for the given system, as shown in Table II.

The fault survey identified a total of 18 possible end-winding interturn fault locations. We applied faults at these locations and checked the protection operation. The results are shown in Table III.

TABLE III
END-WINDING INTERTURN FAULT RESULTS

Element	Number of Faults Detected (higher is better)
87G	NA
32Q	18
59GN	18
50SP	18
87SP	6
87SF	18
67QF	18

We summarize the sensitivity of the various elements to interturn faults as follows:

- 59GN and 87SF provide similar, high sensitivity. The sensitivity of all the instrument transformer and relay errors ($3V_0$, I_2, and I_{f2}) is three turns for this system.
- 32Q has slightly lower sensitivity because of the terminal PTs requiring slightly higher pickup supervision.
- 50SP and 87SP either gain or lose sensitivity depending on the faulted branch because there is a 0.4 percent steady-state circulating current.
- 67QF barely detects a ten-turn interturn fault; the sensitivity is limited by the resolution of the power calculation.
- 87G is unable to detect interturn faults.

3) Series Faults

We inserted a resistance into one branch of the stator to simulate a series fault. The resistance was varied to check the protection operation. The results are shown in Table IV.

TABLE IV
SERIES FAULT RESULTS

Element	Resistance Detected in Ohms (lower is better)
87G	NA
32Q	0.7
59GN	0.3
50SP	1
87SP	6
87SF	0.7
67QF	2

For reference, the machine X_d value is 3.6 ohms. Typically, the elements in consideration gain series-fault sensitivity with an increase in load current; the results presented correspond to our fully loaded machine model.

The results in Table IV can be summarized as follows:

- 59GN can sensitively detect this condition.
- 32Q and 87SF are limited by the sensitivity of the negative-sequence current pickup. 87SF appears to behave similarly to 32Q but is polarized by I_{f2} instead of V_2.
- 50SP and 67QF are slightly less sensitive than the other elements because of slightly higher thresholds.
- 87SP sensitivity does not necessarily increase or decrease with load current. For heavy loads, the element has too much restraint; for light loads, the element does not see a sufficient operating signal. The overall sensitivity is lower than that of the other elements.
- 87G is unable to detect this condition.

While 59GN exhibits superior sensitivity for our system, it is frequently supervised by an element (such as 32Q), thereby incurring a sensitivity penalty. We did not consider an adaptive 50SP pickup that varies with slow seasonal variations to the standing circulating current; the change in pickup can be addressed by relay learning algorithms or operating procedures.

It is challenging to detect a single-turn fault. The protection element sensitivities we chose for evaluation were set as low as we considered reasonable. Good protection philosophy should consider adequate security margins in addition to sensitivity requirements based on a machine survey. As mentioned earlier, based on this philosophy, the main protection schemes for two different types of machines in the Three Gorges generating plant are different to provide optimal coverage for each machine type [12] [16].

V. Conclusion

Conventional phase fault protection using generator phase differential elements can detect a large number of internal faults involving multiple phases, but it is unable to detect interturn, interbranch, and series faults. If protection for these fault types is needed, one of the other elements evaluated in this paper should be considered.

We modeled internal asymmetric faults for a small generator using the multi-loop method and evaluated the sensitivity performance of various protection schemes. The multi-loop method is an approach that considers the nonuniform permeance and winding functions of the machine to obtain circuit parameters and solves the resulting loops. The approach is intuitive because it represents the physical coil inductances moving with respect to each other, but it can be difficult to implement because it requires accurate machine data and a good understanding of the method. The method is likely worth pursuing for the evaluation of protection schemes for large, critical units. Performing a survey of the stator winding is always a good idea to obtain a general idea of the protective requirements for the machine. Unlike some of the other approaches to machine modeling, the multi-loop method allows for a detailed protection scheme evaluation by modeling internal faults on any machine branch. However, a further evaluation of scheme performance with respect to security is required.

We did not validate our model for all fault types, and there may be unobserved inaccuracies; we plan to address this in the future through staged fault testing on a large utility generator. In addition, we plan to enhance our model by adding a damper-winding model, simplifying the model to use machine data that are easier to obtain, facilitating the application of rotor interturn faults, and considering generator control system responses.

VI. Appendix A: Air-Gap Permeance

The derivation for air-gap permeance is given in [5]. Here, we provide a simplified representation of the results. The salient-pole rotor structure with its relevant geometric parameters is shown in Fig. 1.

We can define the air-gap permeance coefficient, $\lambda_\delta(x)$, as follows:

$$\lambda_\delta(x) = \frac{\mu_0}{\delta(x)} \tag{44}$$

where:

$\lambda_\delta(x)$ is the permeance per unit area; also called the permeance coefficient.

μ_0 is the permeability constant.

$\delta(x)$ is the air-gap length as a function of rotor position.

The air-gap permeance under a pole face has a period of π electrical radians, hence it only contains even harmonics. The general expression of the permeance coefficient is shown in (1) (repeated here for convenience):

$$\lambda_\delta(x) = \frac{\lambda_0}{2} + \sum_l \lambda_{2l}\cos(2lx);\ l = 1, 2, \ldots \tag{45}$$

The Fourier series coefficients in (45) are as follows:

$$\lambda_0 = \frac{4}{\pi}\int_0^{\frac{\pi}{2}} \frac{\mu_0}{\delta(x)}dx \tag{46}$$

$$\lambda_{2l} = \frac{4}{\pi}\int_0^{\frac{\pi}{2}} \frac{\mu_0}{\delta(x)}\cos(2lx)dx \tag{47}$$

For salient-pole machines the normalized (with respect to δ_{min}) air-gap length under the pole face ($0 < x < \alpha\pi/2$) is calculated as follows:

$$\delta_P(x) = 1 + (\rho - 1)\frac{\sin^2\left(\frac{x}{P}\right)}{\sin^2\left(\frac{\alpha\pi}{2P}\right)} \tag{48}$$

$$\rho = \frac{\delta_{max}}{\delta_{min}} \tag{49}$$

where P is the number of pole pairs in the machine.

The air-gap length in the interpolar space ($\alpha\pi/2 < x < \pi/2$) is composed of two parts, one in the d-axis and one in the q-axis, which are calculated as follows:

$$\delta_{di}(x) = \rho\frac{\sinh K}{\sinh K\frac{\pi - 2x}{(1-\alpha)\pi}} \tag{50}$$

$$\delta_{qi}(x)=\rho\left(1+\frac{\tau}{\delta_{max}\pi}\left(x-\frac{\alpha\pi}{2}\right)\cos\frac{\pi}{2P}\right) \quad (51)$$

$$K=0.768\left(\tan^{-1}\frac{(1-\alpha)}{2}\frac{x}{\delta_{max}}\right)\left(\frac{(1-\alpha)}{2}\frac{\tau}{\delta_{max}\pi}\right)^{0.617} \quad (52)$$

The air-gap permeance coefficient is the sum of the contribution from the part under the pole face and the interpolar part (mean permeance from the d-axis and the q-axis), as shown in the following equation:

$$\lambda_{2l}=\frac{4}{\pi}\frac{\mu_0}{\delta_{min}}\left(\int_0^{\frac{\alpha\pi}{2}}\frac{\cos(2lx)}{\delta_P(x)}dx+\frac{1}{2}\left(\int_{\frac{\alpha\pi}{2}}^{\frac{\pi}{2}}\frac{\cos(2lx)}{\delta_{di}(x)}+\frac{\cos(2lx)}{\delta_{qi}(x)}dx\right)\right) \quad (53)$$

Cylindrical rotors are a special case of the salient-pole rotor. With a uniform air-gap length (δ), the resulting air-gap permeance is constant, with a square-wave flux. The permeance coefficient then simplifies to the following equation:

$$\lambda_{2l}=\frac{4}{\pi}\frac{\mu_0}{\delta}\int_0^{\frac{\pi}{2}}\cos(2lx)\,dx \quad (54)$$

VII. Appendix B: Core Saturation

Core saturation is modeled to obtain the operating point, as shown in the following equation, at which point the behavior is considered linear.

$$V_t=K_{hys}\bullet V_{NOM\_LG}\bullet\tan^{-1}\left(\frac{I_{fd}\bullet\omega\bullet M_{fp}}{K_{hys}\bullet V_{NOM\_LG}}\right) \quad (55)$$

K_{hys} is a constant that reflects core saturation behavior. Larger values reflect better core characteristics, resulting in a closer match with the air-gap line. The performance of the model with K_{hys} = 1.6 can be seen in Fig. 13.

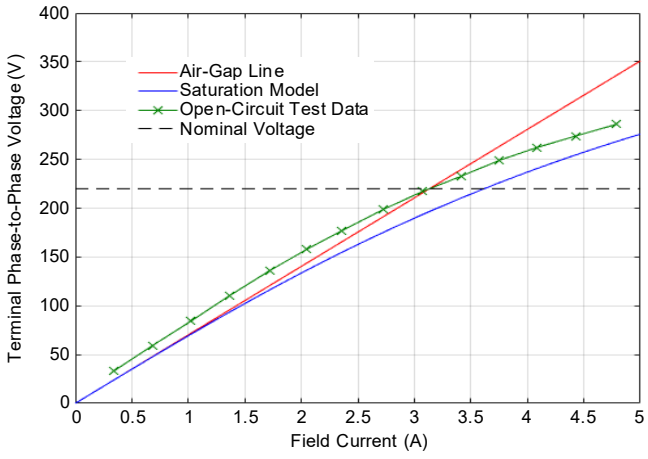

Fig. 13. Performance of the saturation model

When extrapolating the open circuit test data at low values of field current, the voltage does not go through the origin. This is due to core remanence and hysteresis, which are not modeled.

VIII. Appendix C: Machine Data

The relevant machine parameters are summarized in Table V.

TABLE V
MACHINE PARAMETERS

Parameter	Data
Rated power	17.5 kVA
Rated voltage	220 V
Rated current	46 A
Rated power factor	0.80
Nominal frequency	60 Hz
Rated speed	1,200 rpm
Number of pole pairs	3
No-load excitation current	3.14 A
Turns per stator coil	10
Coils per stator branch	9
Branches per stator phase	2
Number of stator slots	54
Stator pitch ratio	7/9

IX. Appendix D: Survey of Fault Types and Locations

We found that the best strategy to obtain the possible end-winding fault locations for our machine was to inspect slots corresponding to a single coil group. The remaining faults were identified by simply extrapolating the phases and locations through the winding. We inspected the winding shown in Fig. 14 to determine the coil layer and slot involved in the fault, then we determined the locations in the stator winding via Fig. 15.

The various fault types under Slot 1 through Slot 3 are shown in Table VI. For instance, the first entry corresponds to a fault between the following two coil locations:

- **T2 (C1_7/9)**: Top (**T**) layer of Slot **2** (Fig. 14).
  This location corresponds to Phase **C**, Branch **1**, Coil **7** of **9** (Fig. 15).
- **B54 (B2_1/9)**: Bottom (**B**) layer of Slot **54** (Fig. 14).
  This location corresponds to Phase **B**, Branch **2**, Coil **1** of **9** (Fig. 15).

This end-winding fault is shown in Fig. 14, and the coil locations involved in the fault are shown in Fig. 15 with fault symbols. Some of the faults in Table VI are invalid (both locations are the same) or are duplicates (point to the same two locations as another pair), hence they have been crossed out.

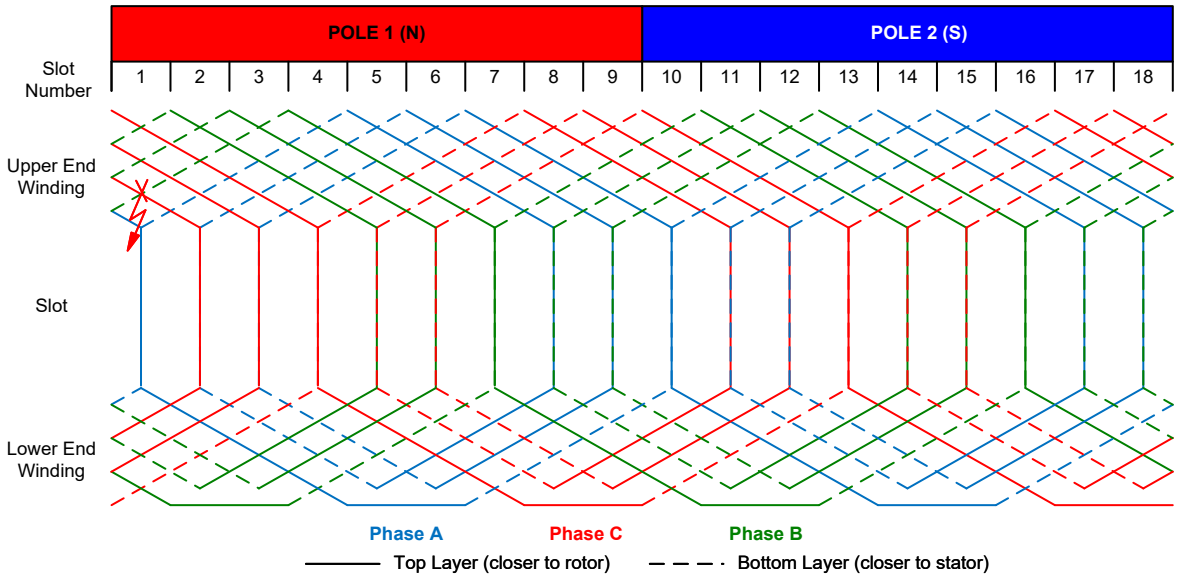

Fig. 14. Stator winding diagram used for survey of fault types in the end-winding region

TABLE VI
SURVEY OF END-WINDING FAULTS FOR A SINGLE COIL GROUP

Slot	Upper End Winding	Lower End Winding
1	T2 (C1_7/9) - B54 (B2_1/9)	~~T2 (C1_7/9) – B54 (B2_1/9)~~
	T3 (C1_8/9) - B53 (B2_2/9)	~~T3 (C1_8/9) – B53 (B2_2/9)~~
	T4 (C1_9/9) - B52 (B2_3/9)	B4 (C2_3/9) – T52 (B1_9/9)
	T2 (C1_7/9) - B01 (A1_0/9)	T2 (C1_7/9) – T1 (A2_0/9)
	T3 (C1_8/9) - B54 (B2_1/9)	~~T3 (C1_8/9) – B54 (B2_1/9)~~
	T4 (C1_9/9) - B53 (B2_2/9)	B4 (C2_3/9) – B53 (B2_2/9)
2	T3 (C1_8/9) – B1 (A1_0/9)	T3 (C1_8/9) – T1 (A2_09)
	T4 (C1_9/9) – B54 (B2_1/9)	B4 (C2_3/9) – B54 (B2_1/9)
	~~T5 (B2_2/9) – B53 (B2_2/9)~~	~~T5 (B2_2/9) – B53 (B2_2/9)~~
	T3 (C1_8/9) – B2 (A1_1/9)	~~T3 (C1_8/9) – B2 (A1_1/9)~~
	T4 (C1_9/9) – B1 (A1_0/9)	B4 (C2_3/9) – T1 (A2_0/9)
	T5 (B2_2/9) – B54 (B2_1/9)	~~T5 (B2_2/9) – B54 (B2_1/9)~~
3	T4 (C1_8/9) – B2 (A1_1/9)	B4 (C2_3/9) – B2 (A1_1/9)
	T5 (B2_2/9) – B1 (A1_0/9)	T5 (B2_2/9) – T1 (A2_0/9)
	~~T6 (B2_1/9) – B54 (B2_1/9)~~	~~T6 (B2_1/9) – B54 (B2_1/9)~~
	T4 (C1_8/9) – B3 (A1_2/9)	B4 (C2_3/9) – B3 (A1_2/9)
	T5 (B2_2/9) – B2 (A1_1/9)	~~T5 (B2_2/9) – B2 (A1_1/9)~~
	T6 (B2_1/9) – B1 (A1_0/9)	T6 (B2_1/9) – T1 (A2_0/9)

There are 26 possible unique faults under the 3 slots corresponding to a coil group, 25 phase-to-phase and 1 single-coil (10-turn) interturn fault. Accounting for the other faults by extrapolating this approach through the winding, we obtained a total of 468 possible end-winding faults (450 phase-to-phase and 18 interturn). For our model to provide results, we had to avoid matrix singularities. Hence, for faults involving branches at the same percentage of the winding, we shifted the location by a couple of turns. This shift likely has a small impact on our simulations and results.

In the slots, there are 108 possible interturn faults, 1 in each slot layer. Given that each coil has 10 turns, the fault could evolve from a single-turn fault up to a maximum of a 10-turn fault.

Finally, we considered the possibility of series faults in any given branch; the main consideration is the series resistance.

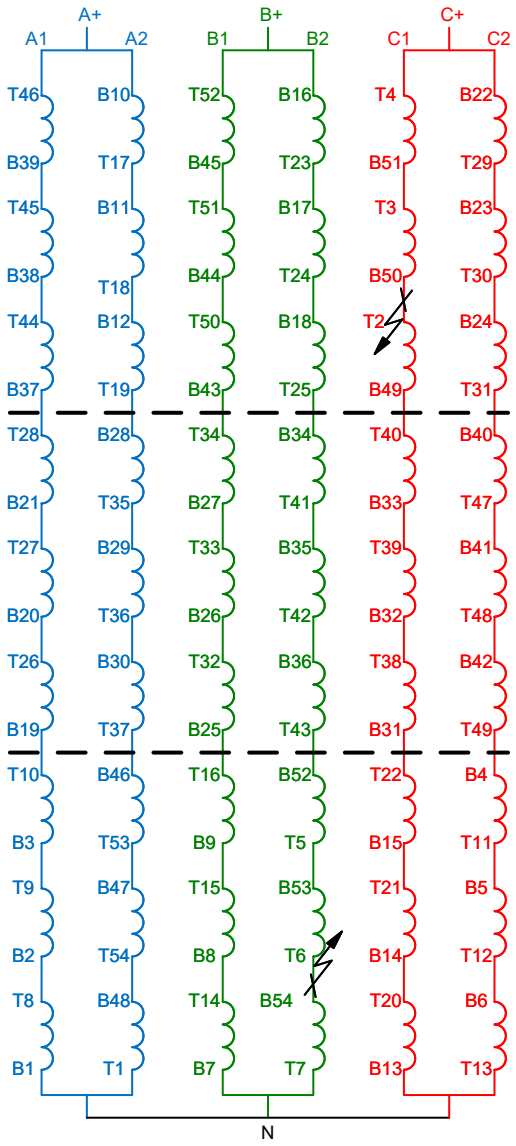

Fig. 15. Location of faults in the stator winding

X. Appendix E: Protection Tolerance to Errors

Protection should be secure from instrument transformer, relay, and transducer measurement errors. This section summarizes a general approximation of these errors, which provide the basis for the element settings.

A. Terminal Voltage

The magnitude error for a single-phase voltage measured by the relay (including relay and PT tolerance) is assumed to be 1 V (1.5 percent) for a 120 V nominal relay (66.7 V line-to-ground). The corresponding error in the sequence quantities is obtained from the errors in the phase voltages ($V_a + \varepsilon$, $V_b - \varepsilon$, $V_c - \varepsilon$). We obtained an error of 1 percent of nominal on the sequence voltages.

If the relay measures $3V_0$, the corresponding error is 1.5 percent; a residual calculation results in a 3 percent error in $3V_0$ (or 1 percent of V_0). In addition, if the neutral voltage is subtracted (instead of wiring the PT neutral to the generator neutral), the associated errors must be considered.

B. Phase Currents

The magnitude error for a single-phase current measured by the relay (including relay and CT tolerance) is 150 mA (3 percent) for a 5 A nominal relay. The corresponding error in the sequence quantities is obtained from the errors in the phase currents ($I_a + \varepsilon$, $I_b - \varepsilon$, $I_c - \varepsilon$). We obtained an error of 2 percent of nominal on the sequence currents.

C. Field Current

The performance of the transducer measuring the field current requires a smaller dynamic range compared with the ac stator currents (during power system faults). Because of the drastic reduction in measurement range, our resolution improved and was in the order of 0.2 percent of the no-load field current (I_{f0}).

XI. Appendix F: Application of 59N to Detect Interturn Faults

A 59N element provides ground fault protection to high-impedance grounded generators. The application of 59N for interturn fault detection for these units requires consideration of the high-impedance capacitive network around the generator.

In the following example, the objective is to detect an interturn fault that shorts 10 percent of the turns of a stator branch. The analysis is done for a high-resistance-grounded machine with a single branch while it is disconnected from the grid. The relevant system parameters are shown in Table VII.

Table VII
Example System Parameters

Generator Rated Voltage	11.5 kV_{LN} (20 kV_{LL})
Nominal Frequency	60 Hz
Capacitances (per phase)	Stator ground (C_G): 0.342 µF External (C_X): 0.100 µF Total: 0.442 µF

The generator neutral grounding resistance in primary ohms is sized as follows:

$$R_N = \frac{1}{3 \bullet \left(2\pi \bullet 60 \bullet 0.442\ \mu F\right)} = 2.0\ k\Omega \qquad (56)$$

The external capacitance (C_X) is mainly composed of the surge capacitor and—to a small extent—the generator step-up unit and the isophase bus. The distributed stator-ground insulation capacitance can be represented as a simplified π-equivalent, as shown in Fig. 16.

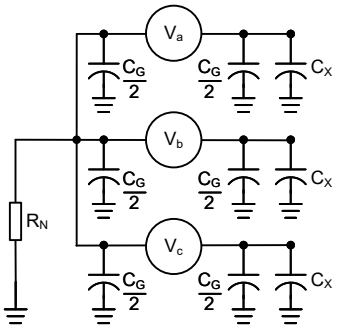

Fig. 16. Generator high-impedance circuit

We simplify the above circuit and represent the equivalent zero-sequence faulted circuit in Fig. 17.

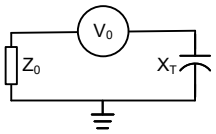

Fig. 17. Simplified zero-sequence circuit of the generator

V_0 is the mean of the phase voltages resulting from the interturn fault.

$$V_0 = \frac{1}{3}\left(V_a + V_b + V_c\right) = 385\ V = 3.3\%\ \text{of}\ V_{LN} \qquad (57)$$

The neutral side impedance imposed is three times the parallel combination of the neutral side capacitance and the grounding resistance.

$$Z_0 = 3 \bullet \left(R_N\ //\ jX_N\right) = 5.6\ k\Omega \angle -21° \qquad (58)$$

$$X_N = \frac{1}{2\pi \bullet 60 \bullet \frac{3C_G}{2}} = 5.2\ k\Omega \qquad (59)$$

The terminal side capacitance is calculated as follows:

$$X_T = \frac{1}{2\pi \bullet 60 \bullet \left(\frac{C_G}{2} + C_X\right)} = 9.8\ k\Omega \qquad (60)$$

The neutral voltage magnitude used by the 59N element can be obtained using the impedance divider principle, as follows:

$$\left|V_n\right| = \left|V_0 \bullet \left(\frac{Z_0}{Z_0 + X_T}\right)\right| = 167\ V = 1.45\%\ \text{of}\ V_{LN} \qquad (61)$$

For a 10 percent interturn fault, 59N measures 1.5 percent of V_{LN} at the neutral. If 59N is set at a typical value of 5 percent (for stator ground fault protection), it should detect an interturn fault that shorts approximately one-third of the stator winding for this system.

A similar analysis approach can be extended to other high-impedance grounded machines with multiple branches connected to the system. The circuit can be solved via superposition with respect to the various sources and impedances.

XII. Acknowledgment

We acknowledge Dr. Reza Iravani from the University of Toronto for his supervision of this work. We thank Doug Taylor, Matchyaraju Alla, and Michael West for sharing data from the scale-model machine.

XIII. References

[1] D. L. Evans, "IEEE Working Group Report of Problems With Hydrogenerator Thermoset Stator Windings Part I – Analysis of Survey," *IEEE Transactions on Power Apparatus and Systems*, Vol. PAS-100, Issue 7, July 1981, pp. 3284–3291.

[2] C. V. Maughan, "Incapability of Analog Relay Protection to Detect Generator Stator Winding Ground Failures at Neutral End," proceedings of the 2013 IEEE Electrical Insulation Conference, Ottawa, ON, Canada, June 2013.

[3] R. H. Park, "Two-Reaction Theory of Synchronous Machines Generalized Method of Analysis – Part I," *Transactions of the American Institute of Electrical Engineers*, Vol. 48, Issue 3, July 1929, pp. 716–727.

[4] P. Krause, O. Wasynczuk, S. Sudhoff, and S. Pekarek, *Analysis of Electric Machinery and Drive Systems, Third Edition*. Wiley-IEEE Press, 2013.

[5] J. Gao, L. Zhang, X. Wang, *AC Machine Systems: Mathematical Model and Parameters, Analysis, and System Performance*. Tsinghua University Press, Beijing, China, 2009.

[6] H. A. Toliyat and T. A. Lipo, "Transient Analysis of Cage Induction Machines Under Stator, Rotor Bar and End Ring Faults," *IEEE Transactions on Energy Conversion*, Vol. 10, Issue 2, June 1995, pp. 241–247.

[7] V. A. Kinitsky, "Mutual Inductances of Synchronous Machines With Damper Windings," *IEEE Transactions on Power Apparatus and Systems*, Vol. 83, Issue 10, October 1964, pp. 997–1001.

[8] P. Subramaniam and O. P. Malik, "Digital Simulation of a Synchronous Generator in Direct-Phase Quantities," *Proceedings of the Institution of Electrical Engineers*, Vol. 118, Issue 1, January 1971, pp. 153–160.

[9] N. A. Al-Nuaim and H. A. Toliyat, "A Novel Method for Modeling Dynamic Air-Gap Eccentricity in Synchronous Machines Based on Modified Winding Function Theory," *IEEE Transactions on Energy Conversion*, Vol. 13, Issue 2, June 1998, pp. 156–162.

[10] A. I. Megahed and O. P. Malik, "Simulation of Internal Faults in Synchronous Generators," *IEEE Transactions on Energy Conversion*, Vol. 14, Issue 4, December 1999, pp. 1306–1311.

[11] P. P. Reichmeider, C. A. Gross, D. Querrey, D. Novosel, and S. Salon, "Internal Faults in Synchronous Machines Part I: The Machine Model," *IEEE Transactions on Energy Conversion*, Vol. 15, Issue 4, December 2000, pp. 376–379.

[12] W. Xiangheng, W. Weijian, and W. Shanming, "Research on Internal Faults of Generators and Their Protection Schemes in Three Gorges Hydro Power Station," proceedings of the Power Engineering Society Winter Meeting, Singapore, January 2000.

[13] H. Liangliang, S. Yuguang, and Q. Ami, "Analysis of the Negative-Sequence Impedance Directional Protection for Stator Internal Fault of Turbo Generator," proceedings of the 2010 International Conference on Electric Machines and Systems, Incheon, South Korea, October 2010.

[14] X. Wang, S. Chen, W. Wang, Y. Sun, and L. Xu, "A Study of Armature Winding Internal Faults for Turbogenerators," *IEEE Transactions on Industry Applications*, Vol. 38, Issue 3, May 2002, pp. 625–631.

[15] X. H. Wang, Y. G. Sun, B. Ouyang, W. J. Wang, Z. Q. Zhu, and D. Howe, "Transient Behaviour of Salient-Pole Synchronous Machines With Internal Stator Winding Faults," *IEEE Proceedings - Electric Power Applications*, Vol. 149, Issue 2, March 2002, pp. 143–151.

[16] W. Shanming, G. Lin, W. Xiangheng, S. Yuguang, W. Weijian, and W. Jianping, "Analysis of Armature Winding Internal Faults and Design of Main Protection Scheme for Synchronous Generators," proceedings of the Eighth IEE International Conference on Development in Power System Protection, Amsterdam, Netherlands, April 2004.

[17] X. Tu, L. Dessaint, N. Fallati, and B. De Kelper, "Modeling and Real-Time Simulation of Internal Faults in Synchronous Generators With Parallel-Connected Windings," *IEEE Transactions on Industrial Electronics*, Vol. 54, Issue 3, June 2007, pp. 1400–1409.

[18] A. B. Dehkordi, "Improved Models of Electric Machines for Real-Time Digital Simulation," Ph.D. thesis, University of Manitoba, 2010.

[19] P. Le-Huy, C. Larose, and F. Figuère, "Flexible Phase-Domain Synchronous Machine Model With Internal Fault for Protection Relay Testing and Related Real-Time Implementation Issues," proceedings of the International Conference on Power System Transients, Delft, Netherlands, June 2011.

[20] A. Banyai, B. Kawkabani, J. Simond, I. Viorel, and L. Vicol, "On the Damper-Bar Current Calculation for High Power Salient Poles Synchronous Machines," proceedings of the 11th International Conference on Optimization of Electrical and Electronic Equipment, Brasov, Romania, May 2008.

[21] H. R. Sills and J. L. McKeever., "Characteristics of Split-Phase Currents as a Source of Generator Protection," *Transactions of the American Institute of Electrical Engineers, Part III: Power Apparatus and Systems*, Vol. 72, Issue 2, January 1953, pp. 1005–1016.

[22] S. Kim, D. Finney, N. Fischer, and B. Kasztenny, "CT Requirements for Generator Split-Phase Protection," proceedings of the 38th Annual Western Protective Relay Conference, Spokane, WA, October 2011.

[23] N. Fischer, D. Finney, and D. Taylor, "How to Determine the Effectiveness of Generator Differential Protection," proceedings of the 67th Annual Conference for Protective Relay Engineers, College Station, TX, March 2014.

[24] *CSC-306 Instruction Manual*, Beijing Sifang Automation Co., Ltd., Beijing, China.

[25] *RCS-985A Instruction Manual*, NR Electric Co., Ltd., Nanjing, China.

[26] B. R. Sunga, T. S. Sidhu, and M. S. Sachdev, "A Modeling Approach for Digital Protection of Synchronous Generators," proceedings of the IEEE WESCANEX 93 Communications, Computers and Power in the Modern Environment Conference, Saskatoon, Saskatchewan, Canada, May 1993.

[27] G. Benmouyal and J. Roberts, "Superimposed Quantities: Their True Nature and Application in Relays," proceedings of the 26th Annual Western Protective Relay Conference, Spokane, WA, October 1999.

[28] B. Kasztenny, A. Guzmán, N. Fischer, M. V. Mynam, and D. Taylor, "Practical Setting Considerations for Protective Relays That Use Incremental Quantities and Traveling Waves," proceedings of the 43rd Annual Western Protective Relay Conference, Spokane, WA, October 2016.

[29] P. M. Anderson, B. L. Agrawal, and J. E. Van Ness, *Subsynchronous Resonance in Power Systems*. The Institute of Electrical and Electronics Engineers, New York, NY, 1990.

[30] IEEE Standard C37.102-2006, IEEE Guide for AC Generator Protection.

[31] *Siprotec 7UM85 Instruction Manual*, Siemens, Munich, Germany.

[32] B. Kasztenny, N. Fischer, H. J. Altuve, "Negative-Sequence Differential Protection – Principles, Sensitivity, and Security," proceedings of the 68th Annual Conference for Protective Relay Engineers, College Station, TX, March 2015.

[33] P. K. Dash, O. P. Malik, and G. S. Hope, “Fast Generator Protection Against Internal Asymmetrical Faults,” *IEEE Transactions on Power Apparatus and Systems*, Vol. 96, Issue 5, September 1977, pp. 1498–1506.

[34] *SEL-221G5 Instruction Manual*, Schweitzer Engineering Laboratories, Inc., Pullman, WA, USA.

XIV. BIOGRAPHIES

Ritwik Chowdhury received his bachelor of engineering degree from the University of British Columbia and his master of engineering degree from the University of Toronto. He joined Schweitzer Engineering Laboratories, Inc. in 2012, where he has served as an application engineer and presently works as a research engineer. He has authored several technical papers on power system protection and control. His interests include the analysis and control of generators and their systems, controlled switching, and generator and line protection. He is a member of IEEE.

Dale Finney received his bachelor of engineering degree from Lakehead University and his master of engineering degree from the University of Toronto. He began his career with Ontario Hydro, where he worked as a protection and control engineer. Currently, Mr. Finney is employed as a senior power engineer with Schweitzer Engineering Laboratories, Inc. His areas of interest include generator protection, line protection, and substation automation. Mr. Finney holds more than 10 patents and has authored more than 30 papers in the area of power system protection. He is a member of the main committee and vice-chair of the rotating machinery subcommittee of the IEEE PSRC. He is a senior member of the IEEE and a registered professional engineer in the province of Nova Scotia.

Normann Fischer received a Higher Diploma in Technology, with honors, from Technikon Witwatersrand, Johannesburg, South Africa in 1988; a BSEE, with honors, from the University of Cape Town in 1993; an MSEE from the University of Idaho in 2005; and a Ph.D. from the University of Idaho in 2014. He joined Eskom as a protection technician in 1984 and was a senior design engineer in the Eskom protection design department for three years. He then joined IST Energy as a senior design engineer in 1996. In 1999, Normann joined Schweitzer Engineering Laboratories, Inc., where he is currently a fellow engineer in the research and development division. He was a registered professional engineer in South Africa and a member of the South African Institute of Electrical Engineers. He is currently a senior member of IEEE and a member of the American Society for Engineering Education (ASEE).

Previously presented at the 2018 Texas A&M Conference for Protective Relay Engineers.

20180119 • TP6825-01